Supporting Information

A Stretchable, Permeable, and Biocompatible Fiber-Reinforced Hybrid Hydrogel Electrode for Highly Stable Electrophysiological Signal Recording

Jinbo Wang[1], Xilin Li[1], Huihe Chen[2], Jingjing Jiang[1], Jieyu Huang[1,3], Jiaxiang Lu[1], Liang Su[1], Shuaikai Xu[1*], Sen Lin[1,3*]

[1]School of Physical Science and Technology, Guangxi University, Guangxi Zhuang Autonomous Region. NO.100, Daxue East Road Nanning, Guangxi Province, 530004, China.

[2]Department of Emergency, Wuming Hospital of Guangxi Medical University, Nanning, Guangxi Province, 530199, China.

[3]Advanced Institute for Brain and Intelligence, Guangxi University, Guangxi Zhuang Autonomous Region. NO.100, Daxue East Road Nanning, Guangxi Province, 530004, China.

*Correspondence to: slin@gxu.edu.cn (Sen Lin); skxu@gxu.edu.cn (Shuaikai Xu); chenhuihe@pku.org.cn (Huihe Chen)

This file includes:

Supporting text

Electrical and mechanical tests

Mechanical strain tests were performed using a flexible electronics tester (Shanghai Prtronic Co., Ltd, China) and an electrochemical workstation (shanghai CH Instruments Co., Ltd, China). During cyclic bending fatigue tests, the electrodes were subjected to a bending angle of 60° at a rate of 40° per second, with an applied voltage of 0.5 V. The linear sweep voltammetry method is used in the tensile electrical performance test, the applied voltage range is set to -0.25 V to 0.25 V.

FEA simulation

The FEA simulation was performed by SIMULIA Abaqus 2023. In FEA simulation, a model of 100×50×5 mm was used to represent the actual FRHH electrode. The elastic modulus of SEBS fibers was calculated as 21.0 kPa, and the elastic modulus of the hybrid hydrogel was calculated as 9.8 kPa by mechanical test results. For boundary, one edge surface of the FRHH electrode was constrained to immobility by locking six degrees of freedom, and relative motion was absent between the entities SEBS fibers and hybrid hydrogel. 30% uniaxial strain and a minimum bending radius of 65 mm were employed to simulate different deformation situations. Deformation behavior of the FRHH obeys Mooney-Rivilin model:

$$W_R = \sum_{i,j=0}^{\infty} C_{ij}(I_1 - 3)^i (I_2 - 3)^j \#(1)$$

where W_R is the strain energy density, I is the deformation tensor, C_{ij} is the material constant.

Permeability tests

In the water permeability test, 10 g of water was added into 4 glass vials, which were then sealed with various materials integrated with adhesive sealants, followed by the initial weighing. The vials were subsequently placed in a 40° C electrical thermal convection drying oven (Shaoxing Supo Instrument Co., Ltd, China). The mass of each vial was measured daily to quantify water evaporation over a continuous period of ten days. The gas permeabilities of three materials were directly measured with an automatic filter material tester (CERTITEST 8130A, TSI, USA).

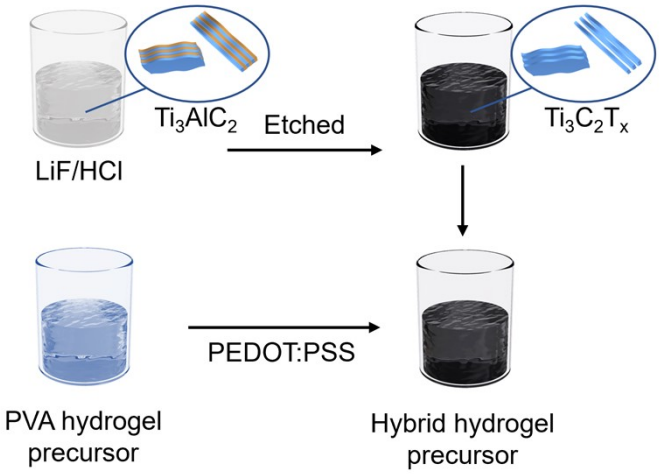

Fig. S1 Schematic diagram of the preparation process of the hybrid hydrogel precursor, including the preparation of PVA hydrogel precursor, dispersion of PEDOT:PSS, etching preparation of $Ti_3C_2T_x$, and their mixing.

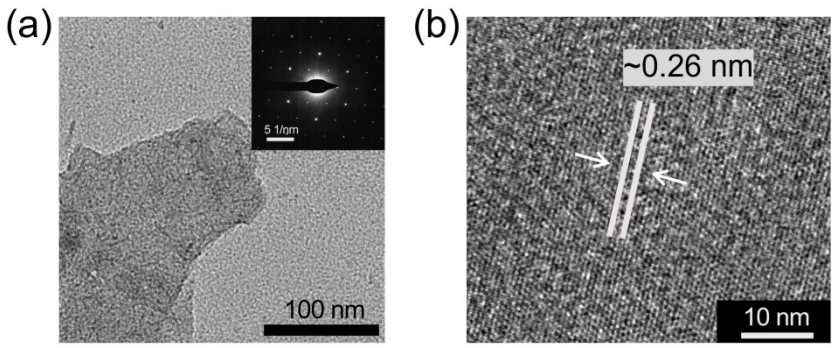

Fig. S2 (a) TEM image of $Ti_3C_2T_x$ nanosheet, the inset showing selected area electron diffraction results, which indicates that the $Ti_3C_2T_x$ nanosheets are highly crystalline single crystals; (b) High-resolution TEM image of $Ti_3C_2T_x$ nanosheet.

Fig. S3 Photograph of (a) the PVA hydrogel precursor, (b) the hybrid hydrogel precursor, and (c) the hybrid hydrogel after crosslinking.

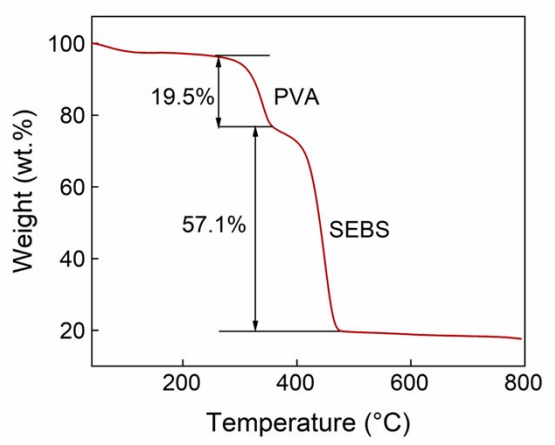

Fig. S4 Thermal analysis results of the FRHH electrode, demonstrating the pyrolysis process of PVA and SEBS.

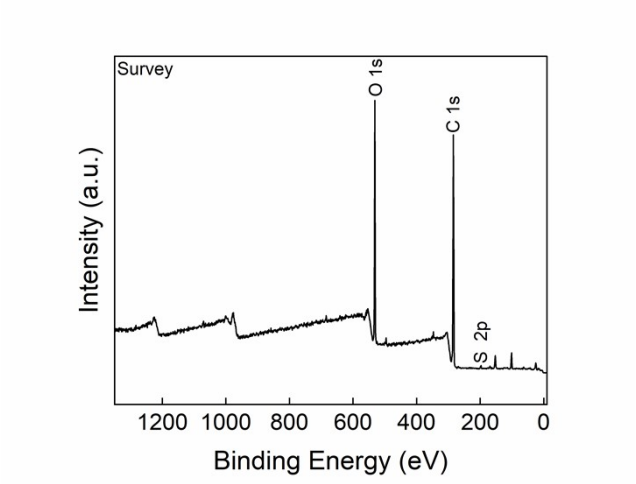

Fig. S5 XPS spectrum of the FRHH electrode.

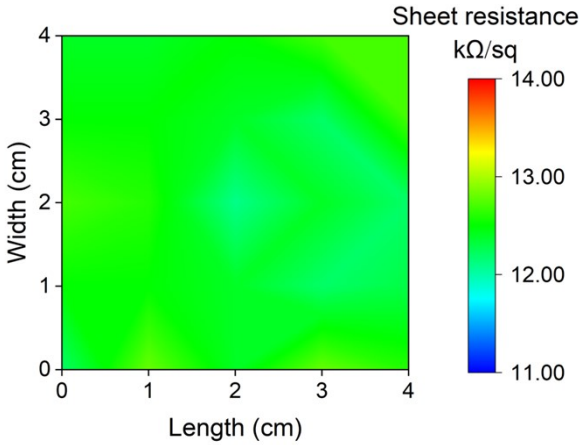

Fig. S6 Sheet resistance of a 4.0×4.0 cm FRHH electrode**.**

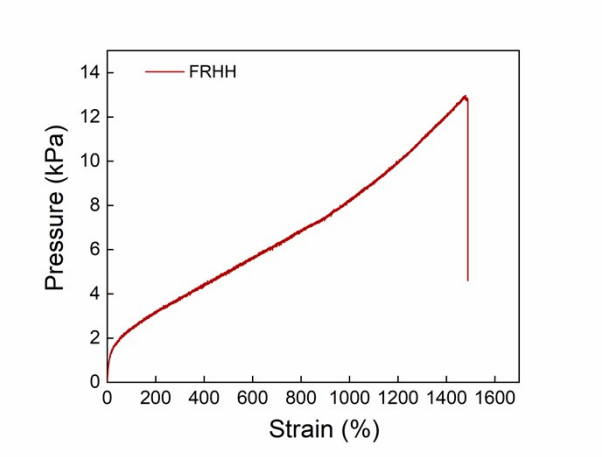

Fig. S7 Fracture strain testing of FRHH electrode with specifications of 3.0×1.7cm.

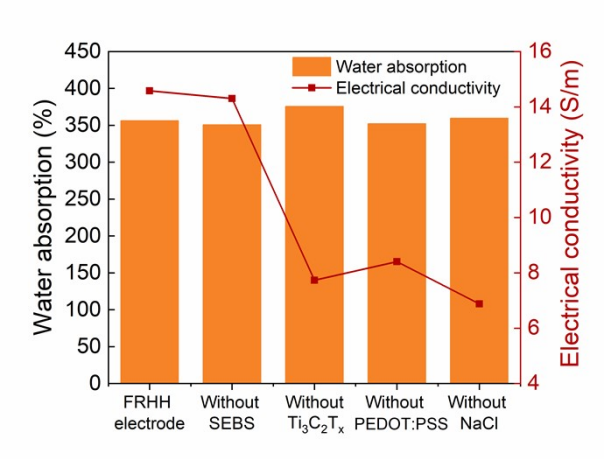

Fig. S8 Water absorption and conductivity test of hydrogels lacking different single components.

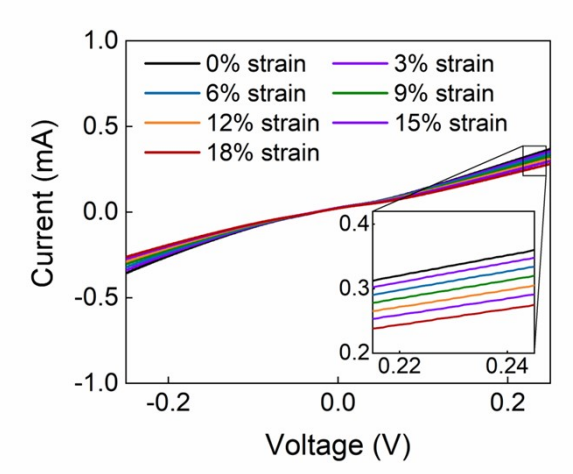

Fig. S9 LSV curves of the FRHH electrode under various strains.

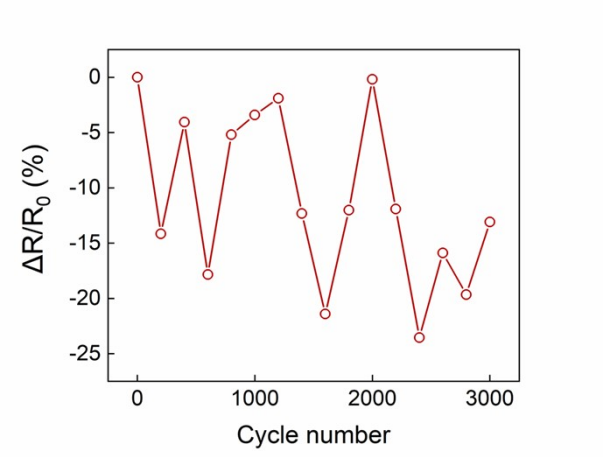

Fig. S10 Resistance change curves of the FRHH electrode during 3000 stretching-release cycles at 25% strain.

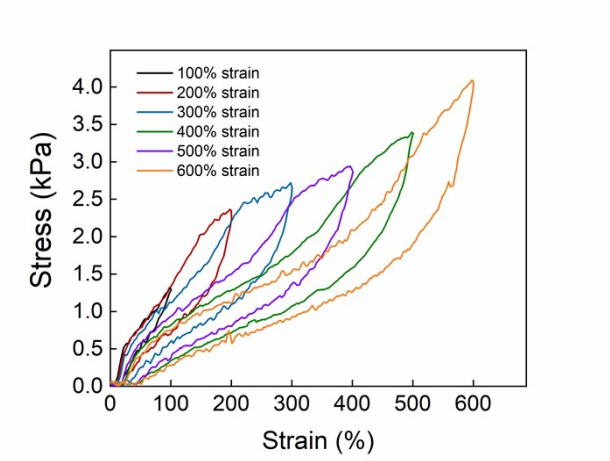

Fig. S11 The uniaxial tensile stress-strain curves of the FRHH electrode under strains ranging from 100% to 600%.

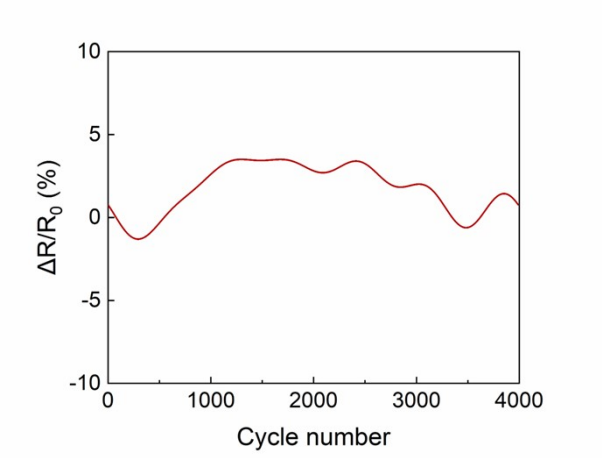

Fig. S12 Resistance change curves of the FRHH electrode during 4000 bending cycles at 40°.

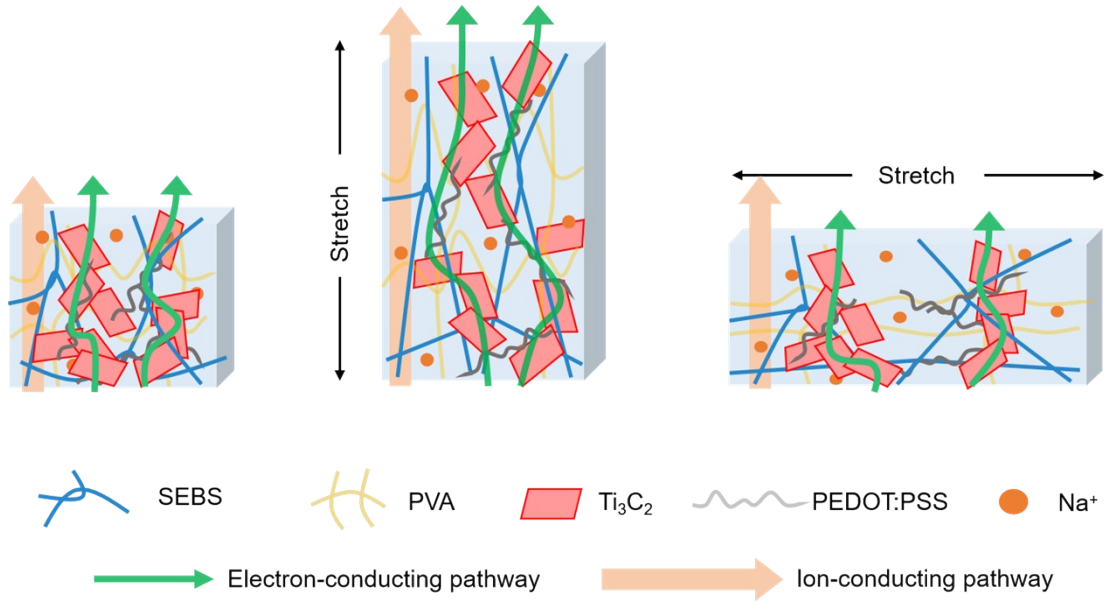

Fig. S13 The conductive schematic diagram during the stretching process of FRHH electrode in different directions.

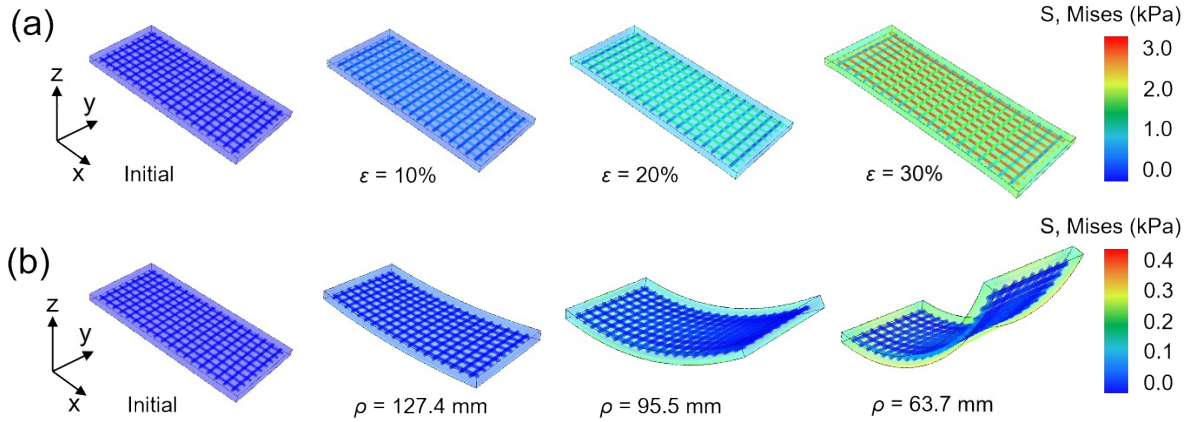

Fig. S14 Finite-element analysis simulation results show the stress distribution of the FRHH electrode under (a) conditions of 10% strain, 20% strain, and 30% strain, and (b) bending conditions with bending radii of 127.4 mm, 95.5 mm, and 63.7 mm.

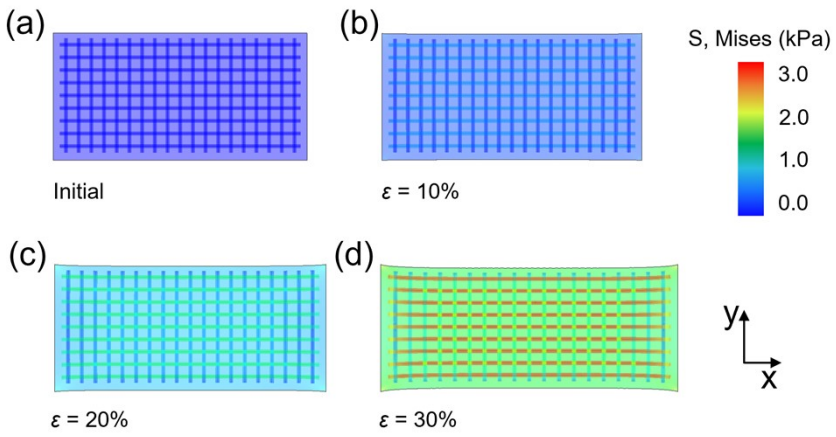

Fig. S15 Front view of FEA simulation of stress distribution in the FRHH electrode under its (a) initial state and uniaxial tension at different strains of (b) 10%, (c) 20%, and (d) 30%.

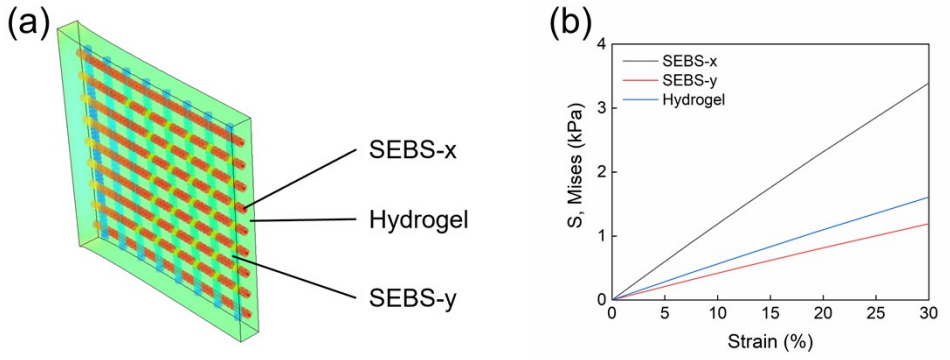

Fig. S16 (a) Cross-sectional view of FEA simulation of the FRHH electrode under uniaxial tension; (b) Stress of the x-direction SEBS fibers, y-direction SEBS fibers, and hydrogel at different strains.

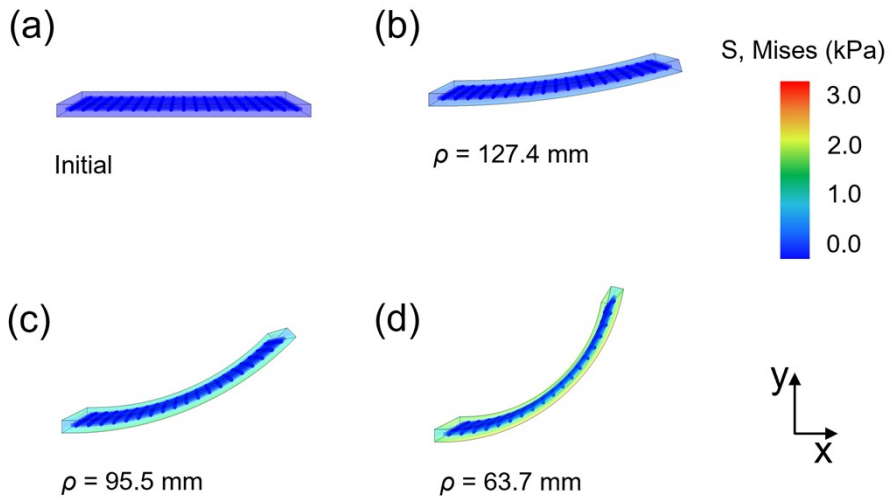

Fig. S17 Front view of FEA simulation of stress distribution in the FRHH electrode under its (a) initial state and bending state with different curvature radius of (b) 127.4 mm, (c) 95.5 mm, and (d) 63.7 mm.

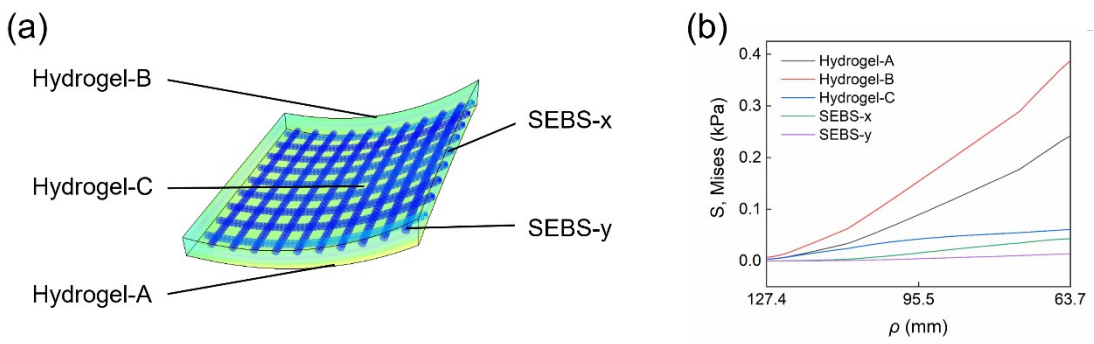

Fig. S18 (a) Cross-sectional view of FEA simulation of the FRHH electrode under bending; (b) Stress of the x-direction SEBS fibers, y-direction SEBS fibers, and the hydrogel on the inner side, outer side, and neutral plane at different curvature radius.

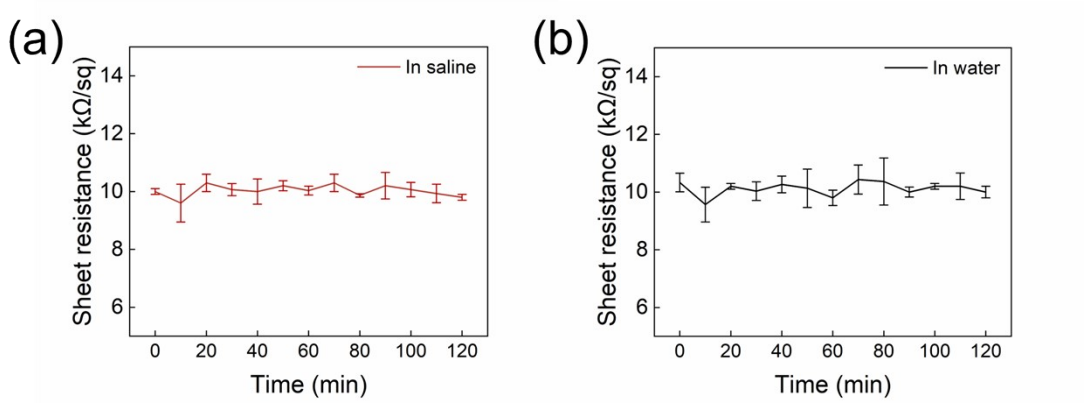

Fig. S19 Stability test of conductivity of FRHH electrode in water (a) and saltwater (b) environments.

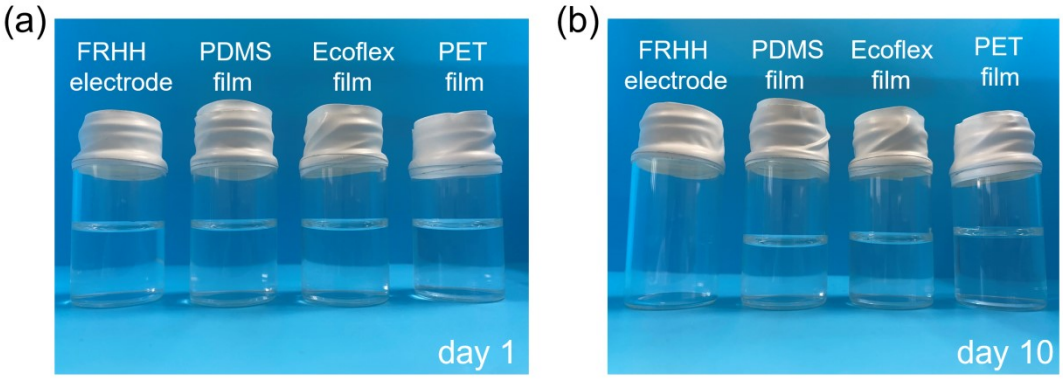

Fig. S20 Photographs illustrating the water permeability tests of different materials at (a) the initial day and (b) after 10 days.

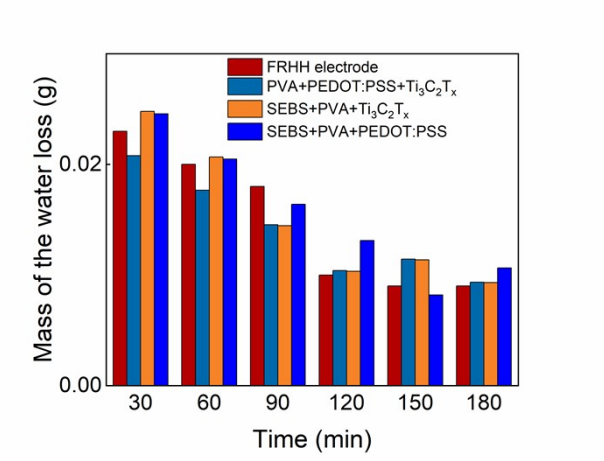

Fig. S21 Water loss test of FRHH electrode and its various component combinations.

Fig. S22 Photograph illustrating the FRHH electrode was soaked and stirred in water for different durations, after which the liquid was extracted for subsequent ICP test.

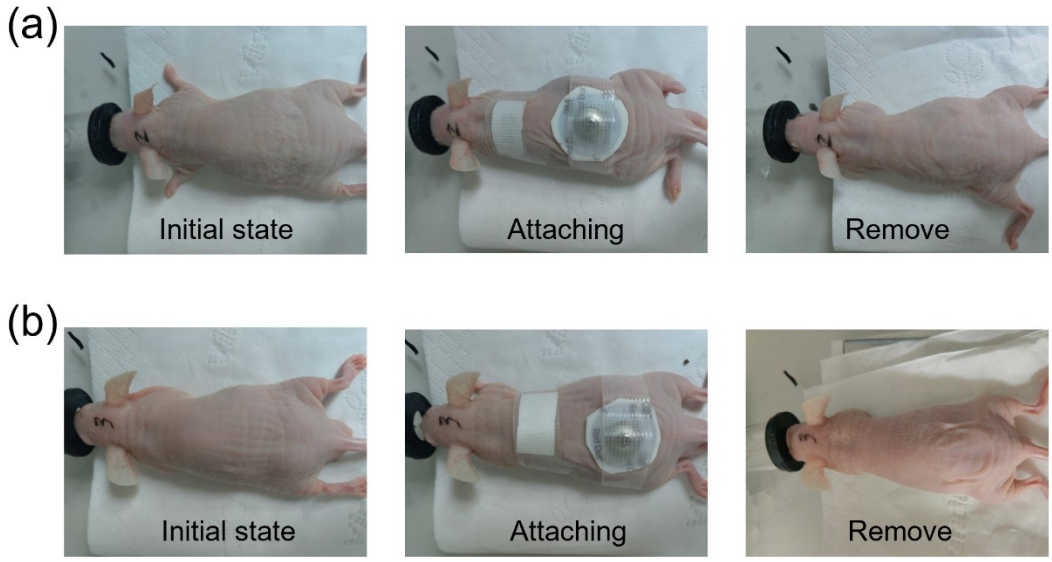

Fig. S23 Photographs of the in vivo biocompatibility tests, where the FRHH electrode and SEBS fiber control group were directly attached on mice's skin and secure with medical tape for (a) 6 h and (b) 2 h.

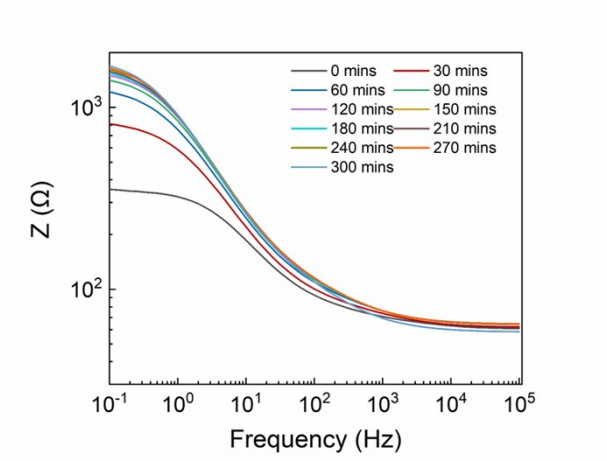

Fig. S24 Impedance spectra of FRHH electrode immersed in physiological saline solution.

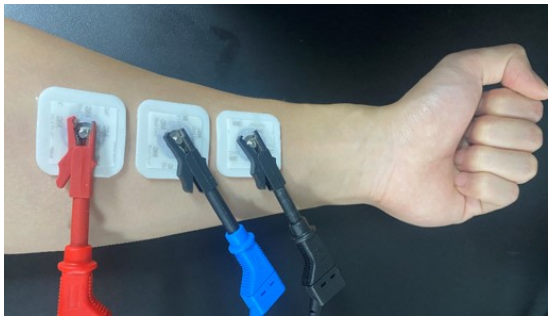

Fig. S25 Photographs of the three-electrode system AC impedance test conducted on human skin, where the red electrode serves as the working electrode, the blue electrode acts as the reference electrode, and the black electrode functions as the counter electrode.

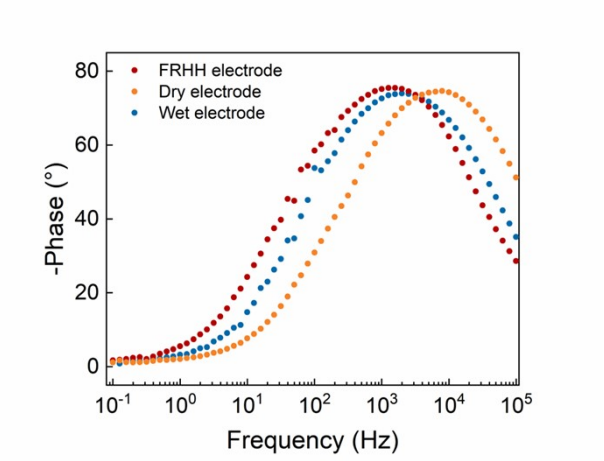

Fig. S26 Phase results of the AC impedance test between three-type of electrodes and skin.

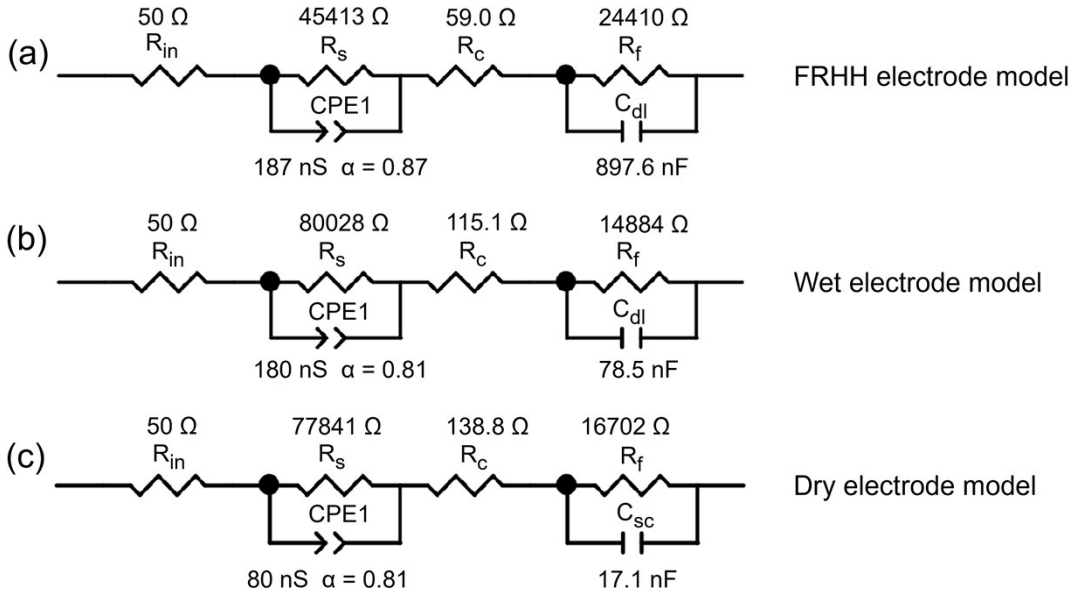

Fig. S27 Equivalent circuit diagrams for the three types of electrode models include (a) FRHH electrode model, (b) wet electrode model and (c) dry electrode model.

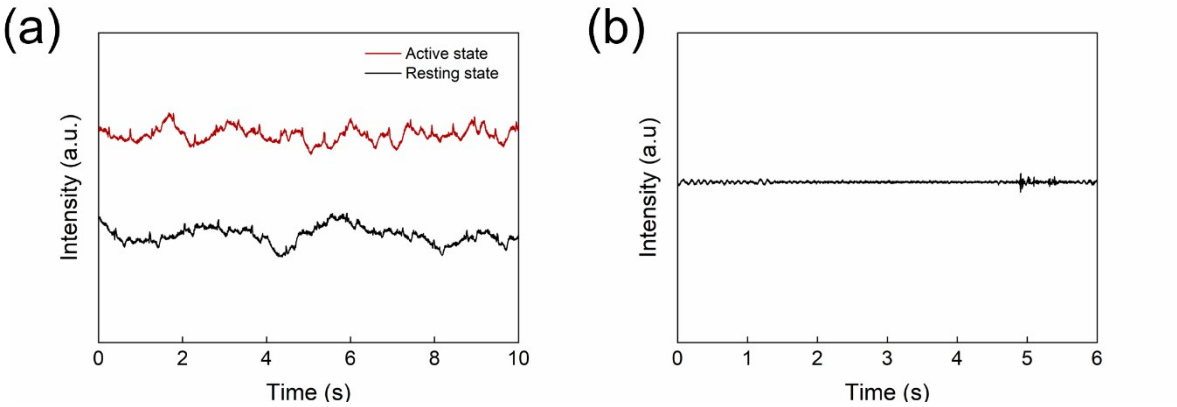

Fig. S28 (a) ECG signals recorded from a subject at rest using the PVA based hydrogel without the conductive fillers. (b) EMG signals acquired from the PVA based hydrogel without the conductive fillers.

Flexible electrode	Impedance at 1000 Hz frequency (Ω)	Fracture strain (%)	Reference
A fiber-reinforced hybrid hydrogel (FRHH) electrode	70	1485%	This work
The hydrogel electronic tattoo (HET) sensors	~20000	300%	Ref. 40
CP-based ionotronics (CPITs) hydrogel	~60	~17%	Ref. 41
The injectable, conductive, adhesive, anti-swelling (ICAA) hydrogel	~100	~180%	Ref. 42
A printable, adhesive, integrative on-skin, and naturally sourced hydrogel with tunable property (PAINT)	~200	88-159%	Ref. 43
A new conducting polymer hydrogel (CPH)	~200	-	Ref. 44
A copolymer hydrogel containing 2-acrylamido-2-methylpropanesulfonic acid (AMPS) and poly(acrylic acid) (PAA)	~400	-	Ref. 45
An asymmetrical bilayer hydrogel EEG electrode	~200	~280%	Ref. 46
The triple-network hydrogel with high-molecular-weight PEG (TN-H)	~200	-	Ref. 47
Improved biocompatible photo-cross-linkable soft hybrid electroactive hydrogels based on gelatin methacryloyol (GelMA) and large area graphene oxide (GO) flakes	~200	-	Ref. 48
The hyaluronic acid-graphite nanoparticles (HAGN) ionic hydrogel	~300	-	Ref. 49

Table. S1 Impedance at 1000 Hz and fracture strain of FRHH and other flexible electrodes.

Video S1. Demonstration of an FRHH electrode illuminating a LED under tensile strain.

Video S2. Demonstration of underwater LED illumination using FRHH electrodes.

Video S3. Demonstration of ECG signal acquisition from a subject in a resting state using FRHH electrodes.

Video S4. Demonstration of ECG signal acquisition from a subject in an active state using FRHH electrodes.

Video S5. A comparison of EMG signal recording on a subject's arms using FRHH electrode and commercial wet electrode.